



HAL
open science

Effect of small-scale atmospheric inhomogeneity on positioning accuracy with GPS

Olivier Bock, Jérôme Tarniewicz, Christian Thom, Jacques Pelon

► **To cite this version:**

Olivier Bock, Jérôme Tarniewicz, Christian Thom, Jacques Pelon. Effect of small-scale atmospheric inhomogeneity on positioning accuracy with GPS. *Geophysical Research Letters*, 2001, 28 (11), pp.2289-2292. 10.1029/2000GL011985 . hal-03973860

HAL Id: hal-03973860

<https://hal.science/hal-03973860v1>

Submitted on 5 Feb 2023

HAL is a multi-disciplinary open access archive for the deposit and dissemination of scientific research documents, whether they are published or not. The documents may come from teaching and research institutions in France or abroad, or from public or private research centers.

L'archive ouverte pluridisciplinaire **HAL**, est destinée au dépôt et à la diffusion de documents scientifiques de niveau recherche, publiés ou non, émanant des établissements d'enseignement et de recherche français ou étrangers, des laboratoires publics ou privés.

Copyright

Effect of Small-Scale Atmospheric Inhomogeneity on Positioning Accuracy with GPS

Olivier Bock,¹ Jérôme Tarniewicz,² Christian Thom,² Jacques Pelon³

Abstract. Global Positioning System (GPS) measurements through a field of km-size atmospheric boundary layer (ABL) inhomogeneities with a 10-ppm index of refraction excess have been simulated and inverted. Biases of up to 1-2 cm in height, 1-5 mm in horizontal, and ~5 mm in zenith tropospheric delay (ZTD) are found, in either static or dynamic atmospheres, using 24-h solutions and estimating ZTD parameters. For 1-h sessions the scatter can increase by a factor of up to 5. These biases are attributed to the inadequacy of standard mapping functions. The use of numerical weather prediction (NWP) models and additional sounding techniques is discussed as a means of improving mapping functions. Raman lidars are thought to offer the highest potential for this purpose and for external calibration of both hydrostatic and wet path delay.

1. Introduction

Tropospheric path delay is recognized as a major error source in geodetic GPS positioning, limiting the accuracy in the vertical coordinate to about 5-10 mm [Davis *et al.*, 1985; Ware *et al.*, 1993; Dodson *et al.*, 1996]. In standard GPS data analysis, ZTD parameters are estimated along with station coordinates. The variation in path delay with elevation angle is usually modeled with mapping functions which assume an azimuthally symmetrical atmosphere [Niell, 1996]. In the presence of horizontal gradients in the temperature and water vapor fields, RMS errors in station heights of 8-10 mm can arise [Ichikawa *et al.*, 1996; Chen and Herring, 1997; MacMillan and Ma, 1998]. Atmospheric turbulence is usually considered to produce random fluctuations with some spatial correlation. Estimating either path delay gradient parameters from the GPS data or using turbulent atmosphere models has been shown to improve only slightly the positioning accuracy [Dodson *et al.*, 1996; Chen and Herring, 1997; Bar-Sever *et al.*, 1998; Emaradson and Jarlemark, 1999].

¹Ecole Supérieure des Géomètres et Topographes / CNAM, Le Mans, France.

²Laboratoire d'Optoélectronique et Microinformatique / IGN, Saint Mandé, France.

³Service d'Aéronomie / CNRS, Université Pierre et Marie Curie, Paris, France.

Copyright 2001 by the American Geophysical Union.

Paper number 2000GL011985.
0094-8276/01/2000GL011985\$05.00

When long term geodetic processes are studied, the combination of 24-h solutions is a means of smoothing out most of the atmospheric effect. This, obviously, cannot be done in applications such as GPS leveling and the determination of geoid height corrections, where a high vertical accuracy (~ 1 mm) is required from short (1-h) observing sessions. There, GPS might offer a quick and convenient alternative to the time-consuming classical leveling. However, atmospheric effects must be investigated more thoroughly and processing strategy revised.

2. Small-scale atmospheric processes

Several different atmospheric processes are active over 1-h time scales: rolls, thermals, and small-scale turbulence [LeMone, 1976]. Small-scale turbulence produces random fluctuations in water vapor density and temperature with spatial scales of < 100 m temporal scales of seconds. In convective ABLs, some steady atmospheric features, such as thermals (km-scale eddies) and rolls (organized large eddies), result from the merging of turbulent processes [Stull, 1988]. Thermals are eddies of sizes 100 m-1 km with time scales of 10-30 min. They rise from the ground to the top of the boundary layer (0.5-2 km), and are often distributed with wavelengths of 1-2 km. They show temperature and humidity deviations of 0.2-2 K and 0.2-1 g/kg, respectively [Lenschow and Stephens, 1980]. They translate very slowly, horizontally, with a velocity of 70-80% that of the mean wind [Stull, 1988]. Thermals can merge into rolls, which are then roughly aligned with the mean wind direction and can persist over even longer times [LeMone, 1976]. Rolls develop in the whole vertical extent of the ABL and their horizontal size is about 2-10 times the vertical. They are typically separated by 2-8 km in the horizontal and can extend up to 500 km in length [LeMone, 1976]. They usually exhibit temperature and humidity deviations of 0.5-3 K and 0.5-3 g/kg, respectively [Weckwerth *et al.*, 1996].

3. Simulation approach

According to these observations, we have investigated the effect of 1-km diameter spherical eddies with a refractivity excess of $\Delta n = 10$ ppm (e.g., a variation in specific humidity from 7 g/kg to 8.5 g/kg or in relative humidity from 57 % to 70 % at 15°C). The path delay excess through the diameter of a sphere is thus $\epsilon_{\Delta\phi} = 1$ cm. Note that we investigated only the effect refractivity inhomogeneities and not the effect of total

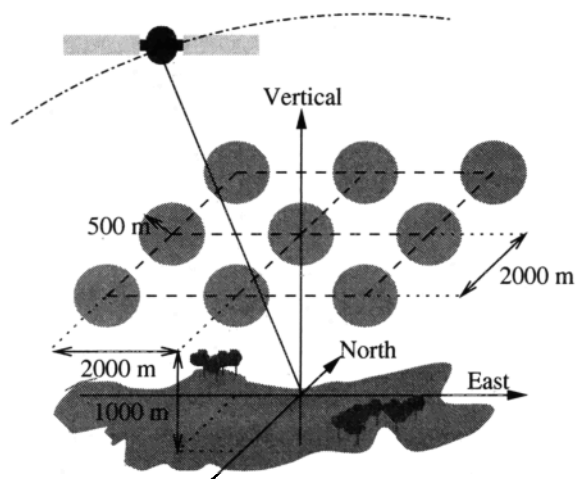


Figure 1. View of the simulated atmospheric inhomogeneities (1 km-size eddies).

refractivity. These latter have been extensively been studied in the past (e.g., [Santerre, 1991]).

A number of eddy distributions, at a height of 1 km, have been considered (see Figure 1): (1) a single eddy at zenith, (2) a single eddy 1 km to the south, (3) a set of nine eddies distributed on a regular grid with a horizontal spacing of 2 km, (4) an extension of case 3 in the E-W direction (three infinite rows of eddies), (5) identical to case 4 with an offset of 250 m to the south. The first three distributions are static, while the two latter are dynamic with a horizontal speed of 2 m/s.

GPS data have been simulated and inverted using either a simplified least-squares method described in [Santerre, 1991], or the Bernese 4.0 software [Rothacher and Mertvart, 1996], for a typical mid-latitude sky distribution. The former is very similar to the method used by Emaradson and Jarlemark [1999], and might be extended to gradient atmospheric models [Bar-Sever et al., 1998]. It easily allows to simulate different satellite sky distributions and the effect of elevation cutoff angle, ζ_{max} . It assumes a uniform satellite sky distribution, which is actually not the case, even for a 24-h session, but has the advantage of producing results which are independent of the time of observation. Since in our study it was also important to investigate 1-h sessions, we also used the Bernese software which, in addition, allowed for the estimation of more than one ZTD parameter per session.

4. Results

We first analyze the three static cases, for which data have been simulated and inverted using the simplified method. Figure 2a and 2b show station height errors, ε_H , as a function of ζ_{max} , either with or without a ZTD parameter estimated. In all three cases, ε_H is about a factor of 3-5 higher when ZTD is estimated. We attribute this effect to the inadequacy of the mapping function to model the angular variation of the simulated path delay. When a ZTD parameter is estimated, the

path delay is assumed to vary roughly as $\sec\zeta$. This is obviously not the case in the presence of the simulated inhomogeneities. As a result, estimated ZTDs (see Figure 3), and other correlated parameters such as clocks and station heights, are strongly biased. The positive errors in ZTD are partly responsible for the large negative errors in station height.

Note that the error in ZTD is about 5 mm at $\zeta_{max}=75^\circ$, which would convert to an error in precipitable water vapor of ~ 1 mm [Bar-Sever et al., 1998; Emaradson and Jarlemark, 1999].

In case 1, and $\zeta_{max}=75^\circ$, $\varepsilon_H = -8$ mm without ZTD estimated and -2.5 cm with ZTD estimated. This is in fact the worst case, the eddy at the zenith having there the strongest effect on station height (it defines a solid angle about 10 times larger than the farthest eddy of case 3 which contributes to the height error by 2-3 mm only at $\zeta_{max}=75^\circ$).

In cases 1-3, $|\varepsilon_H|$ decreases when ζ_{max} is increased, due to the limited field-of-view of the simulated atmospheric inhomogeneities ($\pm 70^\circ$ in case 3). This behavior differs significantly from the results reported by Santerre [1991] and Herring [1986]. Santerre [1991] simulated a homogeneous layer, which is equivalent to a bias in a priori ZTD. In his case, ε_H increased with ζ_{max} , leading to the well-known relationship of $\varepsilon_H \approx 3 \times \varepsilon_{ZTD}$ at $\zeta_{max}=75^\circ$. Estimating a ZTD parameter in his case removes all the bias in station height, since path delay variation is then properly modeled with a $\sec\zeta$ mapping function. Herring [1986] simulated the effect of random path delay fluctuations, with no angular correlation. He showed that the scatter in station height increases with decreasing ζ_{max} , and is amplified when ZTD parameters are estimated. His conclusions are somewhat similar

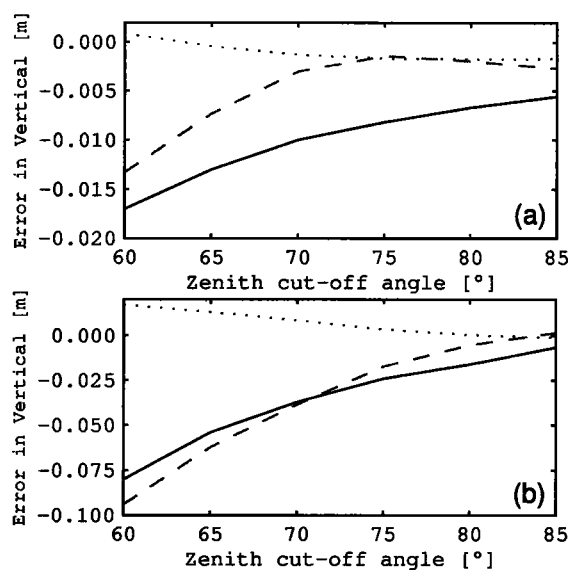


Figure 2. Error in vertical as a function of zenith cut-off angle ζ_{max} (solid line for one eddy at zenith, dotted line for one eddy 1 km at south, dashed line for nine eddies), (a) no ZTD estimated and (b) with a ZTD parameter estimated.

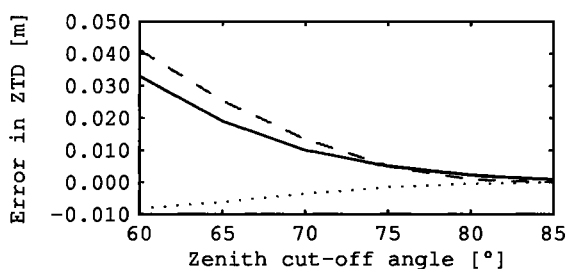


Figure 3. Error in estimated ZTD (solid line for one eddy at zenith, dotted line for one eddy 1 km at south, dashed line for nine eddies)

ours, though we investigated the effects of quasi-steady or correlated path delay errors.

In an asymmetric atmosphere, errors arise also in the horizontal coordinates. In case 2, an eddy is located toward the south, producing thus an error in the north component. Figure 4 shows ϵ_N as a function of ζ_{max} , with $\epsilon_N=2.2$ mm at $\zeta_{max}=75^\circ$. It is interesting to note that these results are independent of whether ZTD is or is not estimated.

The simulations presented above have been confirmed with the Bernese 4.0 software, for $\zeta_{max}=75^\circ$. This second approach has been used to perform simulations and inversions of the dynamic cases 4 and 5 over a 24-h session, and to investigate the results with 1-h sessions and with more than one ZTD parameter estimated per 24-h session. As we expected, additional ZTD parameters did not change the results.

In case 4, the eddies moved from west to east with a 2-m/s velocity. There, one might expect the inhomogeneities to behave as turbulence over a 24-h session and to smooth out. This actually happens only when no ZTD parameter is estimated. When a ZTD parameter is estimated we find $\epsilon_H=-9$ mm. In case 5, all the eddies are offset by 250 m to the south. There we find $\epsilon_H=2.2$ mm with no ZTD parameter estimated and -4.8 mm with one ZTD parameter estimated. The atmospheric asymmetry is then also responsible for an error in horizontal of $\epsilon_N \sim 1.4$ mm.

The amplification of biases when a ZTD parameter is estimated can, again, be attributed to the large deviation of the simulated atmosphere from the modeled one. However, one must notice that spherical inhomogeneities represent probably the worst case with respect to the implemented mapping functions. A further step in this study will be the use of more realistic refractivity fields, such as obtained by large eddy simulations [Stull, 1988], and experimental verification.

Figure 5a and b show the errors in all three coordinates, ϵ_N , ϵ_E , and ϵ_H , for 1-h sessions. Data have been simulated in the asymmetric case 2, at $\zeta_{max}=75^\circ$. The scatter in the results is striking: $\epsilon_N=-0.5-6$ mm, $\epsilon_E=-0.6-2.2$ mm, and $\epsilon_H=-2.5-2.5$ mm, when ZTD is not estimated (Figure 5a). The results do not change in ϵ_N and ϵ_E when ZTD is estimated, but ϵ_H rises to -3.5-14.5 mm.

5. Discussion

We have demonstrated the necessity of using correct mapping functions when estimating ZTD parameters from GPS data. However, this is impossible for the wet path delay, other than on a statistical basis, since the humidity component of the atmosphere is varying quite randomly from day to day. For this reason, the reduction of positioning errors is usually achieved by long term averaging. But this is not applicable for short observing sessions. For the latter, external path delay calibration is required.

For the wet path delay calibration, pointed water vapor radiometers (WVRs) are commonly used. Ware et al. [1993] have shown that using pointed WVR measurements vs. zenith measurements and mapping functions improved the vertical precision by a factor of nearly 2 (from 5.4 to 2.6 mm). They also demonstrated station height repeatabilities as low as 1.2 mm over short baselines (<50 km) and daily solutions [Alber et al., 1997]. However, WVRs are usually used in a total external path delay calibration approach, where the hydrostatic path delay is calibrated from surface pressure measurements. The accuracy in the vertical is about 1/3 of the accuracy in total path delay at the lowest elevation angle [Niell, 1996]. Surface pressure must then be measured within < 0.4 mb to reach a vertical accuracy of ~ 1 mm. This approach might thus fail in the case of asymmetrical atmospheres (horizontal gradients).

Positioning accuracy might be further improved by combining external calibration for the wet path delay and estimation of zenith hydrostatic delay (ZHD) parameters from the GPS data. Therefore, data from NWP models might be used to model the actual mapping function. MacMillan and Ma [1998] have shown that with a gridded ($2^\circ \times 2.5^\circ$) atmospheric data assimilation model, hydrostatic path delay could be retrieved within $< 4.6 \text{ mm} \pm 6-7 \text{ mm}$ at a 5° elevation angle, i.e., a station height accuracy of 1.1 ± 1.7 mm for a 24-h session. This approach might be further improved and possibly hydrostatic path delay might be directly estimated from higher resolution NWP models (~ 10 km). However, with present state of the art NWP models, water vapor inhomogeneities are more difficult to pre-

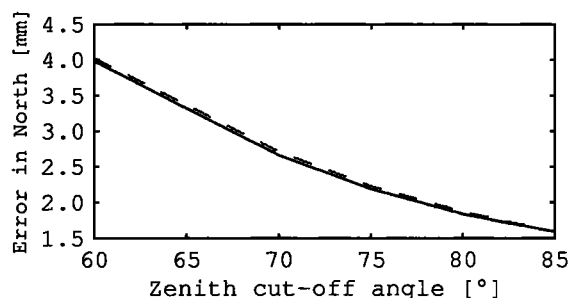


Figure 4. Error in North component for one eddy 1 km at south (solid line no ZTD estimated, dashed line with a ZTD parameter estimated).

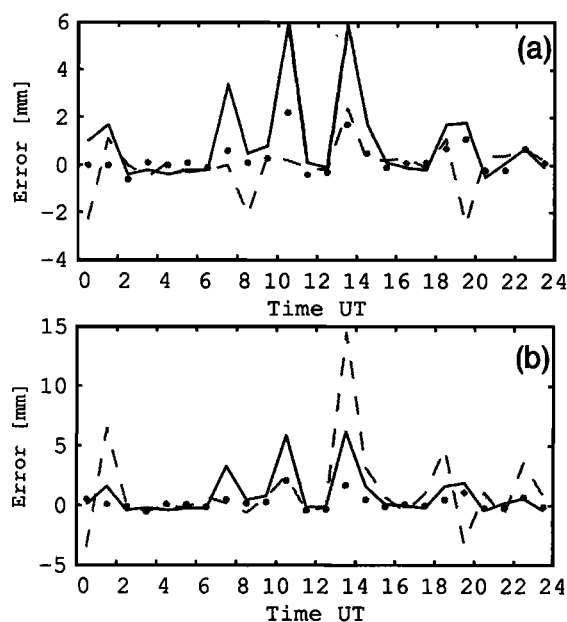


Figure 5. Error in North (solid line), East (dots) and Vertical (dashed), (a) no ZTD estimated, (b) with a ZTD parameter estimated.

dict and biases of a few mm might remain [Ichikawa et al., 1996].

Wet path delay retrieved with WVRs is also limited by the fact that WVRs measure an integrated content rather than profiles. We have evaluated that the diurnal evolution of the lower troposphere can produce errors in WVR-retrieved wet path delay of 5–10 mm [Bock et al., 2001]. These biases might be reduced to 2–3 mm by measuring water vapor profiles, such as provided by Raman lidars [Goldsmith et al., 1998]. Raman lidars also measure air density profiles, from which more accurate hydrostatic mapping function could be derived. In addition, temperature profiles can be retrieved from air density profiles. Such an instrument is presently under development at IGN [Bock et al., 2001]. Efforts are done to achieve profiles with an absolute accuracy of $\sim 1\%$, which might allow for a total external calibration of both hydrostatic and wet path delays. The cost of such an instrument will probably be comparable to that of a WVR. While offering higher accuracy, it will nevertheless have more operational restrictions such as fog, clouds and rain, and probably night time.

References

Alber, C., R. Ware, C. Rocken, F. Solheim, GPS surveying with 1 mm precision using corrections for atmospheric slant path delay, *J. Geophys. Res.*, **24**, 1859–1862, 1997.
 Bar-Sever, Y.E., P.M. Kroger, J.A. Borjesson, Estimating horizontal gradients of tropospheric path delay with a single GPS receiver, *J. Geophys. Res.*, **103**, B3, 5019–5035, 1998.
 Bock, O., Tarniewicz, J., Thom, C., Pelon, J., and Kasser, M., Study of external path delay correction techniques for high accuracy height determination with GPS, *Phys. Chem. Earth* (to be published), 2001.

Chen, G. T.A. Herring, Effects of atmospheric azimuthal asymmetry on the analysis of space geodetic data, *J. Geophys. Res.*, **102**, B9, 20,489–20,502, 1997.
 Davis, J., T. Herring, I. Shapiro, A. Rogers and G. Elgered, Geodesy by radio-interferometry: effects of atmospheric modeling errors on estimates of baseline lengths, *Radio Sci.*, **20**, 1593–1607, 1985.
 Dodson, A. H., P. J. Shardlow, L. C. M. Hubbard, G. Elgered and P. O. J. Jarlemark, Wet tropospheric effects on precise relative GPS height determination, *J. Geod.*, **70**, 188–202, 1996.
 Emardson, T.R., P.O.J. Jarlemark, Atmospheric modelling in GPS analysis and its effect on the estimated geodetic parameters, *J. Geod.*, **73**, 322–331, 1999.
 Goldsmith, J.E.M., F. Blair, E. Bisson, D.D. Turner, Turnkey Raman lidar for profiling atmospheric water vapor, clouds, and aerosols, *Appl. Opt.*, **37**, 4979–4990, 1998.
 Herring T.A., Precision of vertical position estimates from very long baseline interferometry, *J. Geophys. Res.*, **91**, 9177–9182, 1986.
 Ichikawa R., et al., Positioning error in GPS measurements due to atmospheric excess path delay estimated from three-dimensional numerical prediction model data, *J. Geod. Soc. Japan*, **42**, 183–204, 1996.
 LeMone, M.A., Modulation of turbulence energy by longitudinal rolls in an unstable boundary layer, *J. Atmos. Sci.*, **33**, 1308–1320, 1976.
 Lenschow D.H., P.L. Stephens, The role of thermals in the convective boundary layer, *Bound.-Layer Meteor.*, **19**, 509–532, 1980.
 MacMillan, D.S., C., Ma, Using meteorological data assimilation models in computing tropospheric delays at microwave frequencies, *Phys. Chem. Earth*, **23**, 97–102, 1998.
 Niell, A., Global mapping functions for the atmosphere delay at radio wavelengths, *J. Geophys. Res.*, **101**, 3227–3246, 1996.
 M. Rothacher, L. Mertvart (editors), Bernese GPS Software Version 4.0, Astronomical Institute, Univ. Berne, 1996.
 Santerre, R., Impact of GPS satellite sky distribution, *Manuscr. Geod.*, **16**, 28–53, 1991.
 Stull, R.B., An Introduction to Boundary Layer Meteorology, Chap. 11: Convective mixed layer, (Atmospheric Sciences Library, Kluwer Academic, Dordrecht, The Netherlands 1988).
 Ware, R., C. Rocken, F. Solheim, T. Van Hove, C. Alber, J. Johnson, Pointed water vapor radiometer corrections for accurate Global Positioning System surveying, *Geophys. Res. Lett.*, **20**, 2635–2638, 1993.
 Weckwerth, T.M., J.W. Wilson, R.M. Wakimoto, Thermodynamic variability within the convective boundary layer due to horizontal convective rolls, *Mon. Wea. Rev.*, **124**, 769–784, 1996.

O. Bock, Ecole Supérieure des Géomètres et Topographes / CNAM, 72000 Le Mans, France. (e-mail: olivier.bock@ign.fr)

J. Tarniewicz, C. Thom, Institut Géographique National, Laboratoire d'Opto-électronique et Micro-informatique, 2-4 Avenue Pasteur 94165 Saint-Mandé Cedex, France. (e-mail: jerome.tarniewicz@ign.fr; christian.thom@ign.fr)

J. Pelon, Service d'Aéronomie / CNRS, Université Pierre et Marie Curie, 75252 Paris Cedex, France. (e-mail: jacques.pelon@aero.jussieu.fr)

(Received July 5, 2000; revised February 12, 2001; accepted February 26, 2001.)